IJHSR
ijhighschoolresearch.org
RESEARCH ARTICLE

Photon Transport and Spectral Formation in Accreting Neutron Star Columns: A Monte Carlo Approach

Andrew Gan

Raffles Institution, 1 Raffles Institution Lane, Singapore 575954; ganandrew10@gmail.com

ABSTRACT: We present a Monte Carlo model for radiative transfer in the accretion columns of super-critical X-ray pulsars. The simulation follows individual X-ray photons as they propagate through the dense, magnetically confined plasma, focusing on Compton scattering as the dominant interaction process. The physical setup assumes a cylindrical accretion column characterized by the mass accretion rate, bulk inflow velocity, plasma temperature, and column geometry. Both thermal and bulk Comptonisation are treated self-consistently, and relativistic kinematics is included via Lorentz transformations between the electron and laboratory frames. We explore how variations in density, temperature, and flow velocity affect the emergent photon spectra and angular distributions. The results demonstrate the strong sensitivity of the escaping radiation to local plasma conditions in the sinking region, highlighting the importance of Compton scattering in shaping the observed X-ray emission of accreting neutron stars. This framework provides a basis for future models incorporating magnetic effects, cyclotron scattering, and pair production in highly luminous X-ray pulsars.

KEYWORDS: Physics and Astronomy, Astronomy and Cosmology, Neutron Stars, Accretion, Scattering, Radiative Transfer.

Introduction

Accreting strongly magnetized neutron stars (NSs) manifest themselves as X-ray pulsars (XRPs).[1] In these systems, material from a companion star is accelerated in the gravitational field of an NS and reaches the NS surface with velocity $v \simeq c(R_g/R) \sim 0.5c$, where $R_g \simeq 3\ (M/M_\odot)$ km is the gravitational radius of the NS, and M and R are the mass and radius of the NS, respectively.

At the NS surface, the kinetic energy of the accretion flow is transformed into heat and is emitted predominantly in the form of X-rays. The luminosity of XRPs is related to the mass accretion rate $\dot{M}$ as

$$L = \frac{GM\dot{M}}{R} \qquad (1)$$

and covers a wide range from $\sim 10^{33}$ erg s^{-1}, where it is limited by transition into the propeller state[2] or state of stable accretion from cold recombined disc,[3] and up to $\sim 10^{40}$ erg s^{-1}, where XRPs manifest themselves as ultra-luminous X-ray sources (ULXs).[4]

The strong magnetic field of an NS, which is expected to be $\gtrsim 10^{12}$G in XRPs,[5] shapes the geometry of the accretion flow in a region of size $\sim 10^8$ cm around an NS, which is called the NS magnetosphere. Hot plasma in the magnetosphere follows magnetic field lines and reaches the NS surface in a small region of area $\sim 10^9$ cm^2 located close to the magnetic poles of a NS.

Depending on the mass accretion rate, XRPs operate in two distinct regimes.[6] Sub-critical pulsars, with luminosities below a critical threshold of approximately $L_{crit} \sim 10^{37}$ erg s^{-1}, lack a fully developed radiative shock. In this regime, the infalling matter is decelerated primarily by Coulomb collisions or gas pressure near the surface,[7] and the X-ray emission emerges from a hot spot rather than an extended column. In contrast, super-critical XRPs exceed L_{crit}, at which point radiation pressure dominates the dynamics of the flow. A radiative shock forms several stellar radii above the surface, creating an optically thick accretion column in which photons diffuse sideways and escape through the walls.[6,8,9] The resulting geometry and radiation field are fundamentally different between these regimes.

The accretion column structure in the super-critical case is governed by magnetic confinement, radiation pressure, and gravity. The upper region contains the radiative shock, where the supersonic inflow is abruptly decelerated. Below the shock, the sinking region features dense, slowly settling plasma through which radiation diffuses and interacts extensively with electrons. The emergent X-ray spectrum is shaped in this region, with Compton scattering acting as the dominant radiative process.[10] At sufficiently high plasma temperatures, photon-photon interactions can produce electron-positron pairs, increasing the effective scattering opacity and further modifying the dynamics.[11,12]

The goal of this work is to develop a numerical Monte Carlo code to model radiative transfer of X-ray photons in the sinking region of the accretion column of a super-critical XRP. We focus on the kinematics of Compton scattering, which governs energy redistribution between photons and the hot, partially relativistic electron population. Our approach tracks individual photon histories, incorporating bulk inflow velocities, thermal electron motions, and potential pair creation effects. This allows us to examine how local plasma conditions determine the emergent radiation field and the observable spectra of accreting X-ray pulsars.

DOI: 10.36838/IJHSR87.14

Methods

Physical Framework:

We model a filled accretion column of cylindrical shape located at the magnetic pole of an NS. The geometry is characterized by a base radius d and a height H, the latter potentially extending up to a significant fraction of the NS radius R. The accretion column is assumed to be stationary and uniformly filled with plasma channeled along the magnetic field lines.

The mass inflow rate $\dot{M}$ is treated as a global parameter of the simulation, with values in the range $\dot{M} \gtrsim 10^{17}$ gs^{-1} appropriate for bright, super-critical XRPs. Together with the flow velocity v and the column cross-sectional area $A=\pi d^2$, the local mass density of the plasma is determined by

$$\rho = \frac{\dot{M}}{2\pi d^2 v} \tag{2}$$

where the factor of 2 accounts for the presence of two symmetric accretion columns.

We assume a fully ionized hydrogen plasma, so that the number density of free electrons is directly given by $n_e=\rho/m_p$, where m_p is the mass of the plasma. The number density is crucial because it affects the mean free path of the photon, or the average distance it travels between scattering events, and therefore the frequency of such events occurring:

$$l_{fp} = \frac{1}{2\sigma n_e} \tag{3}$$

where σ is the scattering cross-section, which will be discussed later.

The temperature T of the accretion flow is another key parameter of the model. We assume that electrons and protons are thermally coupled so that both species share the same kinetic temperature. In the plasma rest frame, the particle velocities follow a Maxwell–Boltzmann distribution, which gives the probability of any selected particle having a velocity v at temperature T:

$$f(v) = 4\pi v^2 \left(\frac{m}{2\pi k_B T}\right)^{3/2} \exp\left[-\frac{mv^2}{2k_B T}\right] \tag{4}$$

with the characteristic thermal speed $v_t=\sqrt{3k_BT/m}$. The corresponding cumulative distribution is

$$F(v) = \mathrm{erf}\left(\frac{v}{\sqrt{2}v_t}\right) - \frac{\sqrt{2}}{\sqrt{\pi}}\frac{v}{v_t}\exp\left[-\frac{v^2}{2v_t^2}\right] \tag{5}$$

The distributions given by the above equations are used to randomly select the thermal electron velocity for each scattering event, providing an adequate description of the electron gas for $T \lesssim 40$ keV, where the characteristic electron thermal velocities satisfy $v \ll c$. In this work, we focus on the radiative transfer of X-ray photons through the relatively dense sinking region of the column, where photons undergo multiple scatterings before escaping.

We assume that Compton scattering is the dominant process coupling radiation and matter. This is justified by the high electron temperatures and densities expected in super-critical accretion columns, which render free–free absorption and emission comparatively weak at X-ray energies.[13]

The scattering cross section, which represents the probability of a scattering event taking place, is taken to be the standard non-magnetic Klein-Nishina values, appropriate when the local magnetic field does not strongly quantize electron motion or when we are interested in the zeroth-order effect of Comptonisation. For a photon of energy E = hν scattering off an electron at rest, the total Klein-Nishina cross section is

$$\sigma_{KN} = \frac{3\sigma_T}{4}\left[\frac{1+x}{x^3}\left\{\frac{2x(1+x)}{1+2x} - \ln(1+2x)\right\} + \frac{\ln 1+2x}{2x} - \frac{1+3x}{(1+2x)^2}\right] \tag{6}$$

where $x=E/(m_ec^2)$ is the dimensionless photon energy and $\sigma_T \approx 6.65\times10^{-25}$ cm^2 is the Thomson cross section.[14] In the low-energy limit $x \ll 1$, this reduces to the Thomson value:

$$\sigma_{KN} \approx \sigma_T\left(1 - 2x + \frac{26}{5}x^2 + \cdots\right) \tag{7}$$

Since $x \approx 0$, this value is taken to be equal to σ_T, and used in the calculation of the mean free path.

Aside from the path the photon takes, the simulation also calculates and records how the photon energies are affected by scattering. The change in photon energy during a Compton scattering event depends on both the scattering angle and the electron's initial momentum. For the case of an electron initially at rest, the scattered photon energy E' is given by the standard Compton formula,[14]

$$E' = \frac{E}{1 + \frac{E}{m_ec^2}(1 - cos\theta)} \tag{8}$$

Where θ is the scattering angle in the laboratory frame. This expression shows that the photon loses more energy (larger wavelength shift) for larger scattering angles and for higher initial photon energies.

When the electron is moving in the lab frame with a relativistic velocity v, equation (8) is applied after transforming to the electron's rest frame.[14] The incident photon energy in the electron rest frame is obtained via a Lorentz transformation:

$$E_e = \gamma E(1 - \beta cos\psi) \tag{9}$$

Where $\beta = v/c$, $\gamma=(1-\beta^2)^{-1/2}$, and ψ is the angle between the photon propagation direction and the electron velocity in the lab frame. The scattering is then computed using the same Compton formula in (8), but with E_e as the incoming photon energy. If the scattering angle in the electron rest frame is θ_e, the scattered photon energy in that frame is thus:

$$E_e' = \frac{E_e}{1 + \frac{E_e}{m_ec^2}(1 - \cos\theta_e)} \tag{10}$$

Finally, the scattered photon energy in the lab frame is obtained by transforming E_e' back:

$$E' = \gamma E_e'(1 + \beta cos\psi') \tag{11}$$

where ψ' is the angle between the scattered photon direction and the electron velocity in the electron rest frame. This two-step Lorentz transformation procedure allows consistent treatment of Compton scattering on electrons with arbitrary momenta, which is essential for modelling hot plasmas and relativistic outflows.[14]

Bulk and thermal Comptonisation are included in the framework to investigate the significance of both effects. The bulk velocity of the accretion flow v can reach a substantial fraction of the speed of light, so special-relativistic transformations are applied at each scattering to properly account for Doppler shifts and aberration effects. The combined effect of bulk and thermal electron motions produces complex energy redistribution, which our Monte Carlo approach captures by simulating individual photon trajectories and interactions.

The free parameters of the physical framework are therefore: the base radius d and height H of the accretion column, the mass accretion rate $\dot{M}$, the flow velocity v, and the plasma temperature T. These quantities fully specify the density, electron number density, and velocity distribution of the scatterers, providing the input conditions for the radiative transfer simulation.

Monte Carlo Method:

To model the transport of X-ray photons through the accretion column, we employ a Monte Carlo approach in which individual photon trajectories are followed until they escape. The only interaction process considered is Compton scattering, which dominates under the high-temperature, high-density conditions expected in super-critical XRPs.[13] The relevant cross sections and energy–angle relations are given in the previous section and are used here without approximation.

In each simulation run, 10^3 photons are propagated through the cylindrical column. Their evolution is computed iteratively through the following sequence:

1. ***Photon injection:*** A photon is placed at a random position within the column. Its initial propagation direction is chosen isotropically in the plasma rest frame, and its initial energy E_i is set according to the assumed source spectrum.
2. ***Free path sampling:*** The mean free path l_{fp} is calculated from the local electron density n_e and the cross section σ_T. The actual travel distance l is drawn from an exponential distribution:

$$l = -l_{fp}\log(r) \tag{12}$$

Where r is a random value between 0 and 1.

3. ***Boundary check:*** If the updated photon position lies outside the column geometry, the photon is considered to have escaped, and its final energy and direction are recorded. Otherwise, a scattering event is simulated.
4. ***Scattering event:*** A thermal electron velocity is sampled from the Maxwell–Boltzmann distribution. The total electron momentum is then obtained by combining the sampled thermal velocity with the bulk inflow velocity v of the column. Next, a Lorentz transformation to the instantaneous electron rest frame is performed. The scattering is then computed using the relativistic Compton formula, with two random angles determining the outgoing photon direction. Finally, the scattered photon energy and direction are transformed back to the laboratory frame via the inverse Lorentz transformation, accounting for both bulk and thermal motions.
5. ***Iteration:*** The photon's updated position and energy are used as inputs for the next free path sampling step. The process continues until the photon exits the accretion column or a maximum number of scatterings is reached, to prevent the simulation from running for too long.

For each simulation, we also compute the average energy of the photons that successfully escape the accretion column.

If $E_f^{(i)}$ denotes the final energy of the i-th escaping photon and N is the total number of escaping photons, the mean energy is calculated as

$$\langle E_f \rangle = \frac{1}{N}\sum_{i=1}^{N} E_f^{(i)} \tag{13}$$

To quantify the spectral spread, we additionally evaluate the second moment

$$\langle E_f^2 \rangle = \frac{1}{N}\sum_{i=1}^{N} \left(E_f^{(i)}\right)^2 \tag{14}$$

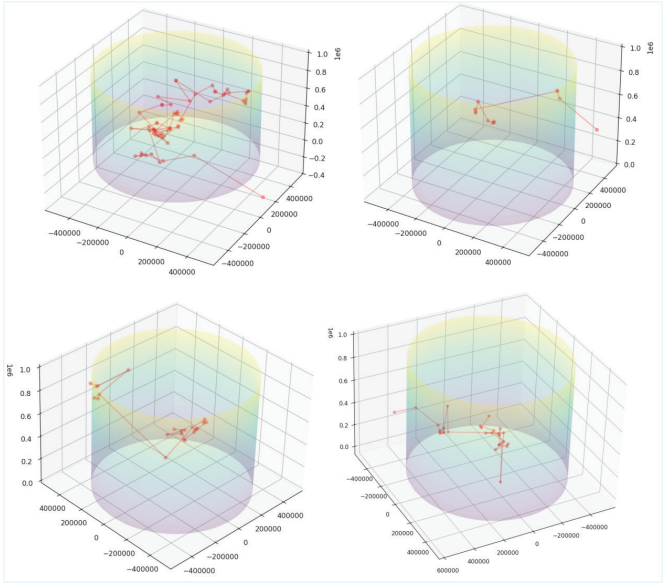

Figure 1: Examples of different photon trajectories inside the accretion column under identical physical conditions. Each dot represents a single Compton scattering event, after which the photon's direction of movement is randomized. The electron number density is artificially reduced for clarity; in reality, the number of scatterings is significantly higher.

which allows us to compute the standard deviation of the emergent photon energies via

$$\sigma_E = \sqrt{\langle E_f^2 \rangle - \langle E_f \rangle^2} \tag{15}$$

These quantities provide a compact measure of the energy redistribution produced by multiple Compton scatterings in the column. For the angular distribution, we also compute the mean final angle θ_f between the photon momentum vector

DOI: 10.36838/IJHSR87.14

and the normal to the neutron star surface, where $0<\theta_f<\pi$. If $\theta_f^{(i)}$ is the final angle of the i-th escaping photon, the average is obtained as

$$\langle\theta_f\rangle = \frac{1}{N}\sum_{i=1}^{N}\theta_f^{(i)} \quad (16)$$

This quantity provides a compact measure of the overall beaming of the escaping radiation relative to the accretion column geometry. This Monte Carlo algorithm naturally incorporates both bulk and thermal Comptonisation as well as special-relativistic Doppler and aberration effects. The resulting ensemble of photon histories yields the emergent angular distribution and energy spectrum for a given set of accretion column parameters. Examples of simulated photon trajectories are shown in Figure 1.

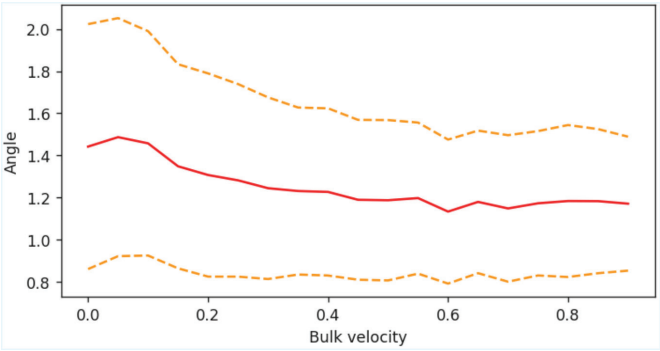

Figure 2: The solid line shows the average angle, in radians, between the normal to the NS surface and the final direction of photon motion for different bulk velocities in terms of c. An angle of $\pi/2$ represents photon escape parallel to the NS.

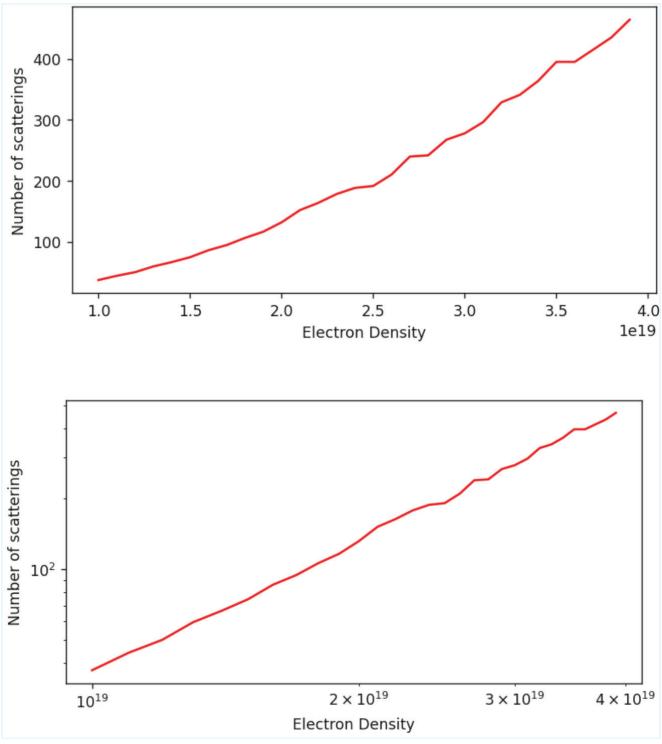

Figure 3: Average number of scatterings for different electron number densities (in cm^{-3}) on linear (top) and logarithmic (bottom) scales.

Results and Discussion

We compute the velocity distribution of electrons, the mean number of scatterings as a function of optical depth, and the spectrum and angular distribution of escaping photons. Additional analysis examines the effect of bulk inflow velocity and the potential contribution of electron– positron pairs to the scattering opacity. Figure 2 demonstrates that the bulk motion of the plasma inside the accretion column strongly affects the final angular distribution of escaping X-ray photons. At high inflow velocities directed towards the neutron star surface, the radiation field becomes increasingly beamed along the direction of the bulk velocity (i.e., downwards) with a lower dispersion, with a significant fraction of photons emerging at angles tilted towards the stellar surface. For all bulk velocities, the average angle $\langle\theta\rangle$ is below $\pi/2$, which reflects the fact that the initial photon source is located near the very bottom of the accretion channel and thus introduces a mild geometric asymmetry even in the static case. The numerical result that increasing β produces a pronounced downward beaming of X-rays is in good agreement with theoretical expectations proposed previously in the literature for super-critical accretion columns.[15-17]

Figure 3 shows the mean number of scatterings as a function of electron density. As expected, increasing n_e reduces the mean free path and significantly raises the number of interactions. This scaling is important in the context of pair creation: under typical accretion column conditions, high-energy photons can generate electron–positron pairs, boosting the scattering opacity. Using the standard low-temperature approximation,18 a temperature $T = 10^9$K yields $n\pm \approx 10^{26}$cm^{-3} , comparable to characteristic electron densities in XRPs, meaning the increase in n_e due to pair creation is non-negligible. The resulting increase in optical depth extends the photon diffusion time and can suppress the emergent luminosity.

The effect of bulk inflow velocity on the scattering statistics is shown in Figure 4. For any fixed density, the mean number of scatterings decreases with β at low velocities and then levels off for $\beta \gtrsim 0.6$. This saturation is a geometric effect: at high inflow speeds, photons are dragged deeper into the column and reflected multiple times from the base before escaping, leading to a quasi-steady mean interaction count. The expected upward trend with density is also evident; higher n_e pushes the system deeper into the optically thick regime, where the Monte Carlo code converges to a diffusion-like limit.

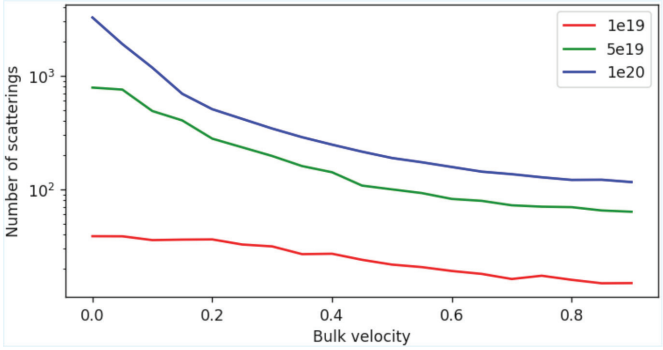

Figure 4: Average number of scatterings as a function of bulk velocity (in terms of c) for different electron densities. The vertical axis is logarithmic.

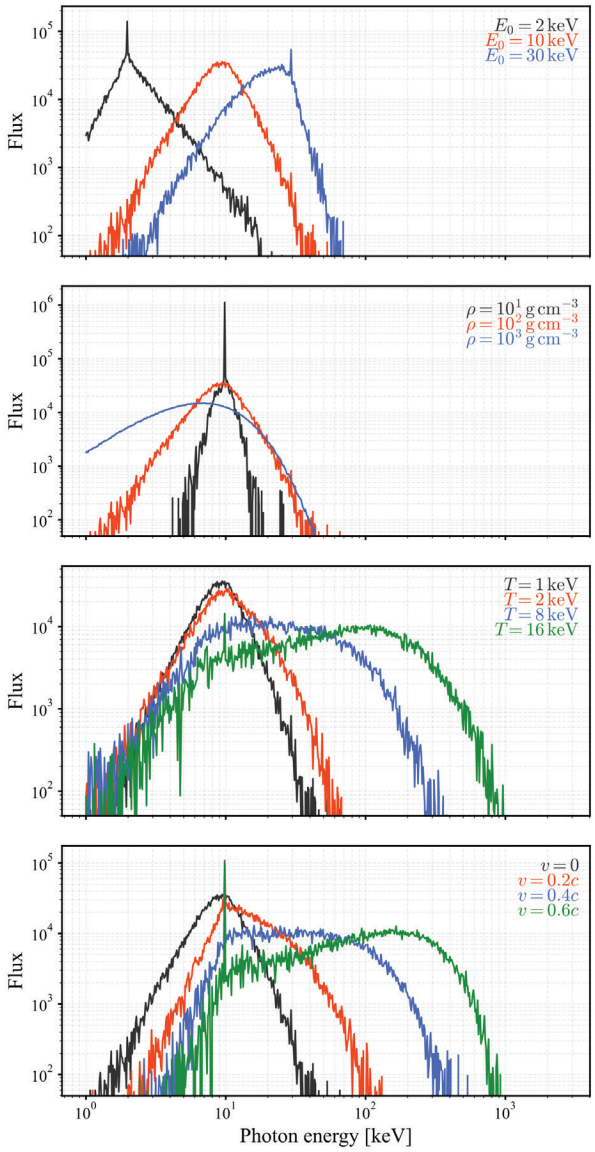

Figure 5: Emergent photon spectra from Monte Carlo simulations of Comptonisation in the accretion column under varying plasma conditions. Both axes are logarithmic. Spectral broadening and hardening are evident in both thermal and bulk Compton regimes.

Figure 5 summarizes the spectral impact of key plasma parameters. The top panel illustrates the dependence on the initial photon energy E_0 : higher E_0 photons retain a larger fraction of their energy and produce extended high-energy tails due to reduced energy loss per scattering and the onset of Klein–Nishina suppression. The second panel shows the effect of density: as ρ increases, the spectrum broadens and approaches a quasi-Wien distribution at ρ = 10^3 gcm^{-3} , indicating near-equilibration with the electron gas. The third panel demonstrates the role of electron temperature: higher T yields systematically harder spectra and shifts the peak to higher energies, in line with expectations from the Kompaneets equation.[14] The bottom panel highlights the impact of bulk inflow: increasing v from 0 to 0.6c causes a clear hardening and energy shift of the spectrum due to bulk Comptonisation, a process distinct from purely thermal scattering. These results confirm that both bulk and thermal Comptonization must be treated simultaneously when modelling super-critical XRPs. The angular redistribution, energy diffusion, and spectral formation are all tightly coupled to the local density, temperature, and inflow velocity in the sinking region of the accretion column.

Conclusion

We have developed a Monte Carlo model to study radiative transfer in the accretion columns of super-critical XRPs, focusing on the role of Compton scattering in shaping the emergent Xray spectra. The Python simulation code was written from scratch specifically for this project and designed to be modular for future extensions. The physical framework assumes a stationary, magnetically confined cylindrical column characterized by the accretion rate, flow velocity, plasma temperature, and geometry. Both bulk and thermal Comptonisation are treated selfconsistently, with full relativistic kinematics included via Lorentz transformations between the electron and laboratory frames.

A Monte Carlo approach was chosen because of its flexibility in handling complex geometries and boundary conditions in the emitting region. This method also allows for straightforward future upgrades to include cross sections that depend strongly on photon energy, propagation direction, and polarization state. A known drawback of the Monte Carlo technique is the increased computational cost in optically thick media due to the large number of scattering events. However, this is partially offset by the ease with which such simulations can be parallelized across multiple processors, making it well-suited for high-performance computing environments.

Our simulations track individual photon histories as they undergo multiple scatterings in the dense sinking region of the column. The results demonstrate that the spectral formation is highly sensitive to the local plasma conditions. In particular:

a) The mean number of scatterings and the angular distribution of escaping photons are strongly dependent on the electron density and the Klein–Nishina cross section, confirming the importance of Comptonisation in optically thick columns.

b) Thermal Comptonization produces systematic spectral hardening as the electron temperature increases, with the emergent spectrum approaching a quasi-Wien distribution at the highest densities.

c) Bulk Comptonization due to coherent inflow at v ~0.1c – 0.6c leads to significant energy amplification, distinct from pure thermal effects, and can shift the entire spectrum toward higher energies.

d) The combined effect of bulk and thermal motions creates complex energy redistribution that cannot be captured by either process in isolation.

e) Multiple scatterings of electrons participating in bulk inflow produce a pronounced downward beaming of escaping X-rays towards the neutron star surface. This behavior, observed in our simulations, is in good agreement with previous theoretical expectations for super-critical accretion columns[15-17] and provides a quantitative framework for modelling the illumination pattern of the stellar surface by the accretion flow.

DOI: 10.36838/IJHSR87.14

f) Pair production at $T \gtrsim 10^9$ K can raise the effective scattering opacity to values comparable to the electron density, prolonging photon diffusion times and reducing the column luminosity.

These findings emphasize that accurate modelling of X-ray pulsar spectra requires simultaneous treatment of both thermal and bulk Compton scattering in the dense sinking region. The beaming effect generated by bulk Comptonisation highlights the need to account for angular redistribution when predicting the geometry of the emitted radiation. Our Monte Carlo approach provides a flexible framework for such studies and can be used in the future to calculate the illumination pattern of the neutron star surface by accretion columns and to link it with observed pulse profiles and surface heating.

Future extensions of this work will incorporate the effects of strong magnetic fields,[19] including quantisation of electron motion and cyclotron resonant scattering, as well as the geometry of fan and pencil beam emission patterns.[20,21] The present results form a baseline for interpreting observations of bright XRPs and ULXs, and for constraining the plasma conditions in their accretion columns.

Acknowledgments

The author would like to thank his mentor, Alexander Mushtukov, for his invaluable guidance during the research project.

References

1. Mushtukov, A.; Tsygankov, S. Accreting Strongly Magnetised Neutron Stars: X-Ray Pulsars. *arXiv (Cornell University)* 2022. https://doi.org/10.48550/arxiv.2204.14185.
2. Illarionov, A. F.; Sunyaev, R. A. Why the Number of Galactic X-Ray Stars Is so Small? *Astronomy and Astrophysics* 1975, *39*, 185–196.
3. Tsygankov, S. S.; Mushtukov, A. A.; Suleimanov, V. F.; Doroshenko, V.; Abolmasov, P. K.; Lutovinov, A. A.; J. Poutanen. Stable Accretion from a Cold Disc in Highly Magnetized Neutron Stars. *Astronomy and Astrophysics* 2017, *608*, A17–A17. https://doi.org/10.1051/0004-6361/201630248.
4. Fabrika, S. N.; Atapin, K. E.; Vinokurov, A. S.; Sholukhova, O. N. Ultraluminous X-Ray Sources. *Astrophysical Bulletin* 2021, *76* (1), 6–38. https://doi.org/10.1134/s1990341321010077.
5. Rüdiger Staubert; Joachim Trümper; Eckhard Kendziorra; D. Klochkov; Konstantin Postnov; Kretschmar, P.; Pottschmidt, K.; Haberl, F.; Rothschild, R. E.; Santangelo, A.; Wilms, J.; I. Kreykenbohm; Fürst, F. Cyclotron Lines in Highly Magnetized Neutron Stars. *Astronomy and Astrophysics* 2019, *622*, A61–A61. https://doi.org/10.1051/0004-6361/201834479.
6. Basko, M. M.; Sunyaev, R. A. The Limiting Luminosity of Accreting Neutron Stars with Magnetic Fields. *Monthly Notices of the Royal Astronomical Society* 1976, *175* (2), 395–417. https://doi.org/10.1093/mnras/175.2.395.
7. Zel'dovich, Ya. B.; Shakura, N. I. X-Ray Emission Accompanying the Accretion of Gas by a Neutron Star. *Astronomicheskii Zhurnal* 1969, *46*, 225.
8. E, L. Y.; A, S. R. Accretion Column Structure. *Soviet Astronomy Letters* 1988, *14*, 390.
9. Wang, Y.-M.; Frank, J. Plasma Infall and X-Ray Production in the Magnetic Funnel of an Accreting Neutron Star. *Astronomy and Astrophysics* 1981, *93*, 255–268.
10. Becker, P. A.; Wolff, M. T. Thermal and Bulk Comptonization in Accretion-Powered X-Ray Pulsars. *The Astrophysical Journal* 2007, *654* (1), 435–457. https://doi.org/10.1086/509108.
11. Mushtukov, A. A.; Ognev, I. S.; Nagirner, D. I. Electron-Positron Pairs in Hot Plasma of Accretion Column in Bright X-Ray Pulsars. *Monthly Notices of the Royal Astronomical Society Letters* 2019, *485* (1), L131–L135. https://doi.org/10.1093/mnrasl/slz047.
12. Suleimanov, V. F.; Mushtukov, A. A.; Igor Ognev; Doroshenko, V. A.; Werner, K. Mean Opacities of a Strongly Magnetized High-Temperature Plasma. *Monthly Notices of the Royal Astronomical Society* 2022, *517* (3), 4022–4033. https://doi.org/10.1093/mnras/stac2935.
13. Frank, J.; King, A.; Raine, D. J. *Accretion Power in Astrophysics*; Cambridge University Press: Cambridge, 2002.
14. Rybicki, G. B.; Lightman, A. P. *Radiative Processes in Astrophysics*; 1986.
15. Kaminker, A. D.; Fedorenko, V. N.; Tsygan, A. I. A Radiating Accretion Column as a Model for an X-Ray Pulsar. *Astronomicheskii Zhurnal* 1976, *53*, 773.
16. Juri Poutanen; Mushtukov, A. A.; Suleimanov, V. F.; Tsygankov, S. S.; Nagirner, D. I.; Doroshenko, V.; Lutovinov, A. A. A REFLECTION MODEL for the CYCLOTRON LINES in the SPECTRA of X-RAY PULSARS. *The Astrophysical Journal* 2013, *777* (2), 115–115. https://doi.org/10.1088/0004-637x/777/2/115.
17. Postnov, K. A.; Gornostaev, M. I.; D. Klochkov; Laplace, E.; Lukin, V. V.; Shakura, N. I. On the Dependence of the X-Ray Continuum Variations with Luminosity in Accreting X-Ray Pulsars. *Monthly Notices of the Royal Astronomical Society* 2015, *452* (2), 1601–1611. https://doi.org/10.1093/mnras/stv1393.
18. Zeldovich, Ya. B.; Novikov, I. D. *Relativistic Astrophysics. Vol 1: Stars and Relativity*; 1971.
19. Harding, A. K.; Lai, D. Physics of Strongly Magnetized Neutron Stars. *Reports on Progress in Physics* 2006, *69* (9), 2631–2708. https://doi.org/10.1088/0034-4885/69/9/r03.
20. Gnedin, Y. N.; Sunyaev, R. A. The Beaming of Radiation from an Accreting Magnetic Neutron Star and the X-Ray Pulsars. *Astronomy and Astrophysics* 1973, *25*, 233.
21. Lutovinov, A. A.; Tsygankov, S. S.; Suleimanov, V. F.; Mushtukov, A. A.; Doroshenko, V.; Nagirner, D. I.; J. Poutanen. Transient X-Ray Pulsar v 0332+53: Pulse-Phase-Resolved Spectroscopy and the Reflection Model. *Monthly Notices of the Royal Astronomical Society* 2015, *448* (3), 2175–2186. https://doi.org/10.1093/mnras/stv125.

Author

Andrew Gan is a high school student at Raffles Institution, Singapore. He has a strong interest in physics and research, which he plans to pursue at university.